Measurement Science
and Technology

PAPER

A new measurement method for the dynamic resistance signal during the resistance spot welding process

To cite this article: Lijing Wang *et al* 2016 *Meas. Sci. Technol.* **27** 095009

IOP Publishing Measurement Science and Technology
Meas. Sci. Technol. **27** (2016) 095009 (12pp) doi:10.1088/0957-0233/27/9/095009

A new measurement method for the dynamic resistance signal during the resistance spot welding process

Lijing Wang[1], Yanyan Hou[1,3], Hongjie Zhang[2,3], Jian Zhao[1], Tao Xi[2], Xiangyang Qi[2] and Yafeng Li[2]

[1] School of Control and Mechanical Engineering, Tianjin Chengjian University, Tianjin 300384, People's Republic of China
[2] Tianjin Key Laboratory of Modern Mechatronics Equipment Technology, School of Mechanical Engineering, Tianjin Polytechnic University, Tianjin 300387, People's Republic of China

E-mail: houyanyan022@163.com and zhanghj022@163.com

Received 19 April 2016, revised 12 July 2016
Accepted for publication 18 July 2016
Published 9 August 2016

Abstract

To measure the dynamic resistance signal during the resistance spot welding process, some original work was carried out and a new measurement method was developed. Compared with the traditional method, using the instantaneous electrode voltage and welding current at peak current point in each half cycle, the resistance curve from the newly proposed method can provide more details of the dynamic resistance changes over time. To test the specific performance of the proposed method, a series of welding experiments were carried out and the tensile shear strengths of the weld samples were measured. Then, the measurement error of the proposed method was evaluated. Several features were extracted from the dynamic resistance curves. The correlations between the extracted features and weld strength were analyzed and the results show that these features are closely related to the weld strength and they can be used for welding quality monitoring. Moreover, the dynamic resistance curve from the newly proposed method can also be used to monitor some abnormal welding conditions.

Keywords: resistance spot welding, dynamic resistance signal, signal processing, feature extraction, correlation analysis

(Some figures may appear in colour only in the online journal)

1. Introduction

Resistance spot welding (RSW) is widely used in the automotive industry [1], however, its welding and joining quality is heavily influenced by various disturbances, such as shunting [2, 3], small edge distance [4], greasy surface [5], poor fit-up [6], electrode wear [7], and so on. In recent decades, many kinds of dynamic signals during the spot welding process have been measured to monitor the spot welding quality, such as welding current [8], welding voltage (electrode voltage) [9], dynamic resistance, electrode force [10],electrode displacement [11–14], sonic emission [15] and temperature [16]. Electrode displacement is one of the most widely used signals for spot welding quality monitoring, but its measurement is inevitably interfered by the displacement sensors with fixtures and parts surrounding welding gun [17]. Wang and Li *et al* [18] found that the electrode displacement curve fluctuations could be used to reflect the weld quality. In their research, an easy-to-install accelemeter was used to measure the displacement vibration instead of the traditional displacement sensor. Dynamic resistance (DR) signal is another widely used signal and it can provide rich information concerning the weld nugget formation and growth [19–21].

A typical spot welding process is schematically shown in figure 1. During the RSW process, DR not only relates to the bulk resistance of the electrodes and sheets, but also the contact resistance at sheet–electrode and sheet–sheet interfaces [22, 23]. In order to measure DR, many methods were

[3] Authors to whom any correspondence should be addressed.

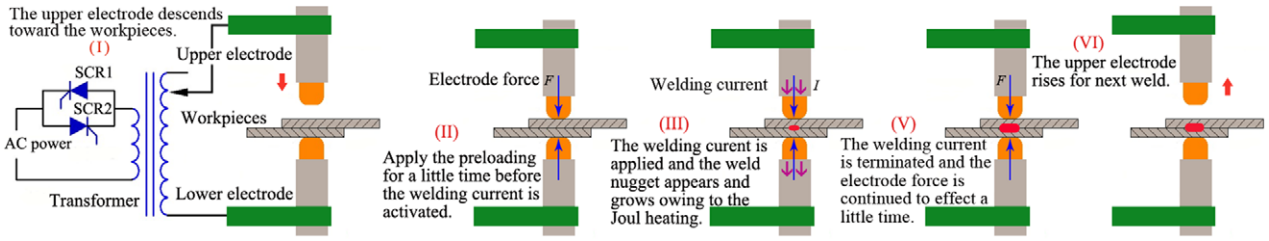

Figure 1. Schematic diagram for the resistance spot welding process.

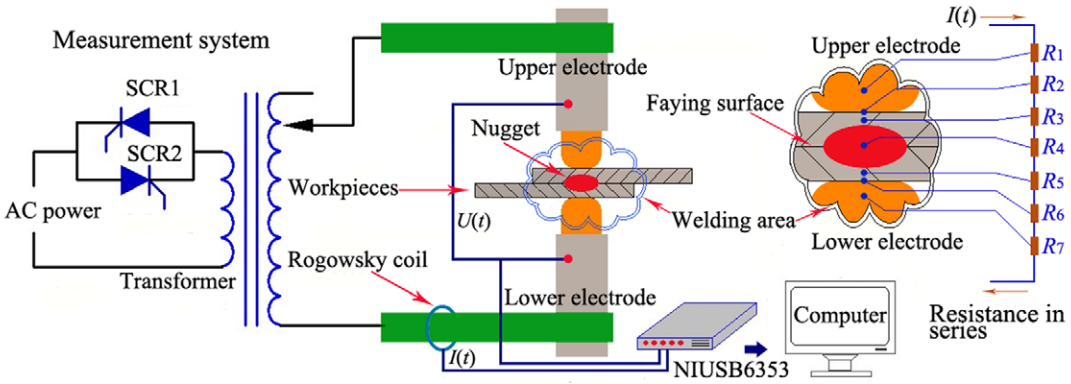

Figure 2. DR measurement system and a detailed description for the dynamic resistance in series.

reported. Savage *et al* [24] and Gedeon *et al* [25] pointed out that DR could be calculated by using the instantaneous welding voltage and current corresponding to the peak current point per half cycle. This method could eliminate the inductive reactance caused by the transformer. Kaiser *et al* [26] calculated DR by dividing the peak voltage by the corresponding peak current in each half cycle. Dickinson *et al* [27] used RMS values of the welding voltage and current per half cycle to calculate DR. Graza and Das [28] utilized a recursive least squares (RLS) algorithm to evaluate the dynamic resistance. Cho and Rhee [29, 30] creatively achieved DR curve from the primary circuit of an AC welding machine. However, the resistance calculation still depended on the voltage and current values corresponding to peak current point in each consecutive half cycle.

So far, the most widely used method for DR calculation is dividing the instantaneous voltage by current at the peak current point. It is believed that this method can remove the inductive noise caused by the transformer. Through connecting the obtained data points together, the DR curve can be obtained. However, the DR curve from this method is highly discrete as the resistance calculation is performed only one time per half welding cycle (i.e. only one resistance data can be obtained in each half cycle). To improve it, some other calculation methods were proposed. Luo *et al* [31] obtained the continuous DR curve by calculating the quotient of the voltage signal and current signal, and the phase shift between these two signals induced by the leakage reactance of the transformer coil was ignored. Another interesting method was reported by Wong and Pang [32], in which the time varying input impedance signal was monitored.

The aim of this study is to develop a new measurement method to acquire the continuous DR signal during the spot welding process. To do this, a measurement system was built and the welding current and electrode voltage were gathered synchronously. Based on the equivalent circuit of the spot welding machine, some new work was carried out. To test the reliability, feasibility and effectiveness of the newly proposed DR measurement method, a series of welding experiments and analysis work were performed. Several features were extracted from the time-domain of the DR curves and the correlations between the extracted features and weld strength were then discussed. Moreover, the DR curves were also used to monitor some kinds of disturbances in the spot welding process.

2. Measurement system and the equivalent circuit of the spot welding machine

To acquire the DR signal during the spot welding process, a measurement system had been developed, as schematically shown in figure 2, where a fixed single phase welding machine (YR-500SA2) was used. Two truncated flat-face electrodes (with the tip diameter of 5 mm) were made of CuCrZr alloy (RWMA class II). In this research, the welding current signal was measured by a Rogowsky coil (PEM CWT60LF) with a sensitivity of 0.5 mV A^{-1}. The voltage was measured using two wire leads attached to the electrode tips. A high performance signal acquisition device (NI USB6363 with ADC resolution of 16 bits) was used to gather the welding current and voltage signals synchronously. The sampling rate was set as 400 kHz.

As the voltage probe cables form a wire loop in the magnetic field created by the alternating welding current, it will induce noise on the welding voltage signal. In order to reduce inductive pickup, a shielded twisted pair wire was used and the input configuration of the signal acquisition device adopted

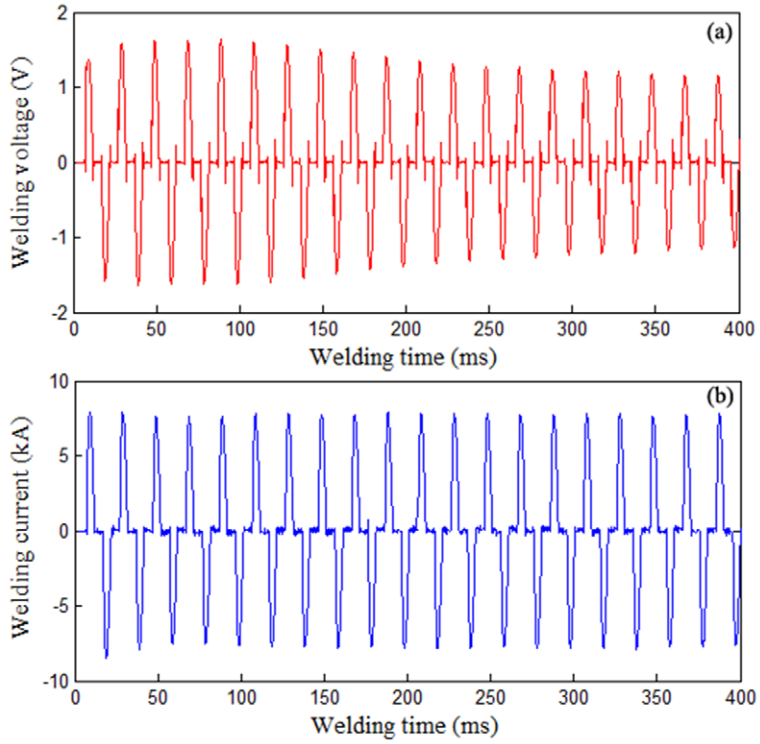

Figure 3. (a) Electrode voltage signal and (b) welding current signal.

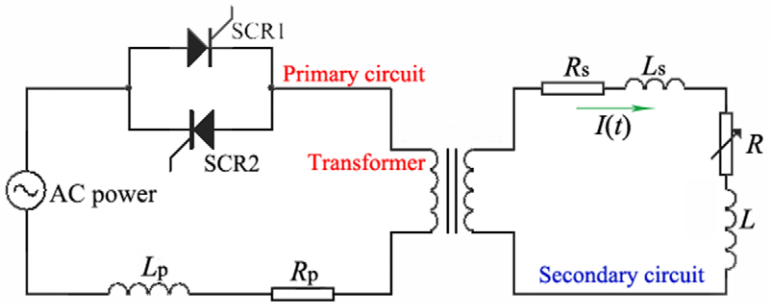

Figure 4. Equivalent circuit of the spot welding machine.

differential connections. Additionally, wavelet de-noising technology was also used to filter the inductive noise. A typical electrode voltage signal with its corresponding welding current signal is shown in figure 3. These two signals were synchronously gathered from a certain welding process with welding current of 5.8 kA.

The electrical circuit of a single phase spot welding machine typically consists of two parallel silicon controlled rectifiers (SCRs) and a transformer, as shown in figure 2. A schematic presentation of this circuit is drawn in figure 4, where R_p and L_p are the equivalent resistance and inductive reactance in the primary coil of the transformer, respectively. R_s and L_s denote the same parameters in the secondary coil. Single loop formed by the welding machine throat also appears as an inductance L in the secondary circuit. R represents the dynamic resistance between the upper and lower electrodes during the spot welding process. A detailed description for this dynamic resistance is shown in figure 2. Before the weld nugget appears, R generally consists of the contact resistance (R_2, R_6 and R_4) and the bulk resistance of the electrodes and sheets (R_1, R_7, R_3 and R_5). Because the contact resistance is much larger than the bulk one at the beginning of the welding process, Joule heat mainly concentrates at the sheet–electrode interfaces and sheet–sheet faying surface, resulting in the fast collapses of the surface asperities and contaminates. As the molten nugget appears and grows, contact resistance R_4 will convert to the bulk resistance of the liquid metal.

Because of the existence of the inductive load in a welding machine circuit, there will be a phase difference between the welding voltage and current signals. To observe this phase shift, welding voltage and current signals (in figure 3) are plotted in one graph, as shown in figure 5(a). A partial enlarged view for the signal segment in the rectangular area in figure 5(a) is provided in figure 5(b), where the phase shift can be seen clearly.

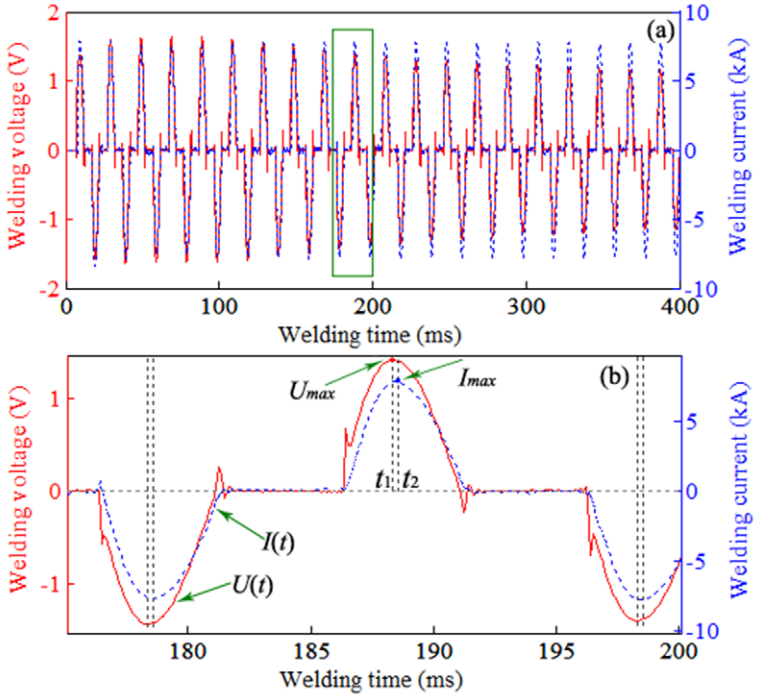

Figure 5. Phase shift between the electrode voltage and welding current waveforms. (a) Voltage and current signals and (b) phase shift between these two signals.

3. Acquisition of the DR curve

Based on the equivalent circuit, the electrical impedance (Z) of the secondary circuit can be expressed as

$$Z = (R + R_s) + j\omega(L + L_s) \tag{1}$$

where ω is angular frequency. Equation (1) also can be written as

$$Z = |Z|(\cos\varphi + j\sin\varphi) = |Z|\,e^{j\varphi} \tag{2}$$

where $|Z| = \sqrt{(R+R_s)^2 + (L+L_s)^2}$. φ ($\varphi = \arctan(\omega L/R)$) is the phase difference between the welding voltage and current, thus, $|Z|\cos\varphi$ is the DR which converts the electrical power to Joule heat. $|Z|\sin\varphi$ corresponds to the dynamic reactance relating to the electrical power conserved in the reactance. In order to calculate the impedance Z, in this research, the raw welding current ($I(t)$) and welding voltage ($V(t)$) signals are firstly converted into the analytic ones by

$$\hat{I}(t) = I(t) + jh[I(t)] \tag{3}$$

$$\hat{V}(t) = V(t) + jh[V(t)] \tag{4}$$

where $h[I(t)]$ and $h[V(t)]$ represent the Hilbert transforms of the welding current signal and voltage signal, respectively. Hilbert transform can be expressed as

$$h[s(t)] = \hat{s}(t) = \frac{1}{\pi}\int_{-\infty}^{\infty}\frac{s(\tau)}{t-\tau}\mathrm{d}\tau \tag{5}$$

Assume that $I(t) = I_m\sin\omega t$, then $V(t) = V_m\sin(\omega t + \varphi)$, thus equations (3) and (4) can be respectively written as

$$\hat{I}(t) = I_m(\sin\omega t - j\cos\omega t) \tag{6}$$

$$\hat{V}(t) = V_m[\sin(\omega t + \varphi) - j\cos(\omega t + \varphi)] \tag{7}$$

Thus the complex electrical impedance of the secondary circuit can be deduced

$$\begin{aligned} Z = \frac{\hat{V}(t)}{\hat{I}(t)} &= \frac{V_m}{I_m}\frac{\sin(\omega t + \varphi) - j\cos(\omega t + \varphi)}{\sin\omega t - j\cos\omega t} \\ &= \frac{V_m}{I_m}\{[\sin(\omega t + \varphi)\sin\omega t + \cos(\omega t + \varphi)\cos\omega t] \\ &\quad + j[\sin(\omega t + \varphi)\cos\omega t - \sin(\omega t + \varphi)\sin\omega t]\} \\ &= \frac{I_m|Z|}{I_m}(\cos\varphi + j\sin\varphi) = |Z|(\cos\varphi + j\sin\varphi) \end{aligned} \tag{8}$$

From equations (2) and (8), it can be confirmed that the real part of the complex electrical impedance just corresponds to the dynamic resistance, while the imaginary part corresponds to the dynamic reactance. Figure 6 shows the DR calculation result (corresponding to the welding process mentioned in figure 3) by taking the quotient of the analytic voltage to current. To remove the sub-harmonic components and avoid the phase distortion caused by the traditional digital filter, FRR zero-phase filtering technology was used.

FRR zero-phase filtering can be realized through four steps [33, 34]. Firstly, the signal data is processed through a causal real-coefficient filter (called first filtering), and then the first filtering output is time-reversed and filtered by the same filter (called second filtering), and finally, the second filtering output is time-reversed again. For the input sample sequence $x(n)$ with the length of $N + 1$, the first filtering output can be written as

$$y_1(n) = x(n) * h(n) \tag{9}$$

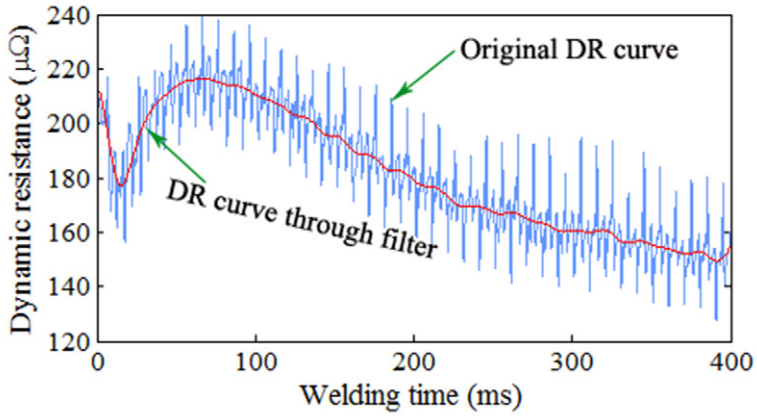

Figure 6. Dynamic resistance signal during spot welding process.

where $h(n)$ is the impulse response sequence of the used digital filter, thus the first time-reversed sequence $y_2(n)$ can be expressed as

$$y_2(n) = y_1(N-n) \tag{10}$$

When $y_2(n)$ is processed through the same digital filter, the filter output $y_3(n)$ is

$$y_3(n) = y_2(n) * h(n) \tag{11}$$

thus, the second time-reversed sequence $y(n)$ is

$$y(n) = y_3(N-n) \tag{12}$$

The expression of the FRR zero-phase filter in frequency-domain can be written as

$$\begin{aligned} Y(w) &= \mathrm{e}^{-j\omega N} Y_3(-\omega) \\ &= \mathrm{e}^{-j\omega N} Y_2(-\omega) H(-\omega) \\ &= \mathrm{e}^{-j\omega N} \mathrm{e}^{j\omega N} Y_1(\omega) H(-\omega) \\ &= Y_1(\omega) H(-\omega) = X(\omega) H(\omega) H(-\omega) \\ &= X(\omega) \left|H(\omega)\right|^2 \end{aligned} \tag{13}$$

where $X(\omega)$, $H(\omega)$ and $Y(\omega)$ respectively correspond to the Fourier transforms of $x(n)$, $h(n)$ and $y(n)$,

From the equation (13), it can be seen that FRR implements a zero-phase filtering with a frequency response $\left|H(\omega)\right|^2$. In this research, a fourth-order digital Butterworth low pass filter was designed and the cut-off frequency was 50 Hz. To inhibit the transient distortion (at the beginning and ending of the filtered signal) induced by FRR method, filter initial state was calculated. Generally, a linear digital filter can be expressed as

$$H(z) = \frac{Y(z)}{X(z)} = \frac{\sum_{k=0}^{M} b_k z^{-k}}{1 - \sum_{k=1}^{N} a_k z^{-k}} \tag{14}$$

where a_k and b_k are the real coefficients of the filter, thus, its corresponding linear difference equation can be written as

$$y(n) = \sum_{k=1}^{N} a_k y(n-k) + \sum_{k=0}^{M} b_k x(n-k) \tag{15}$$

So,

$$\begin{cases} y(m) = b(0)x(m) + z_0(m-1) \\ z_i(m) = b(i+1)x(m) + z_{i+1}(m-1) - a(i+1)y(m) \quad i = 0, \ldots, N-2 \\ z_{N-1}(m) = b(N)x(m) - a(N)y(m) \end{cases} \tag{16}$$

thus the filter initial state z_i of the filter can be calculated by

$$\begin{bmatrix} a(1) & 1 & 0 & 0 & \cdots & 0 \\ a(2) & 0 & 1 & 0 & \cdots & 0 \\ \vdots & \vdots & \vdots & \vdots & & \vdots \\ a(N-1) & 0 & 0 & 0 & \cdots & 1 \\ a(N) & 0 & 0 & 0 & \cdots & 0 \end{bmatrix} \begin{bmatrix} z_0 \\ z_1 \\ z_2 \\ \vdots \\ z_{N-1} \end{bmatrix} = \begin{bmatrix} b(1) - a(1)b(0) \\ b(2) - a(2)b(0) \\ \vdots \\ b(N-1) - a(N-1)b(0) \\ b(N) - a(N)b(0) \end{bmatrix} x(m) \tag{17}$$

The FRR zero-phase filtering result is also shown in figure 6. A generalized DR evolution can be seen clearly: a rapid drop concerning with contact resistance decrease at the early stage of RSW process, a fast rise between the trough and beta peak, and a gradual decline relating to weld nugget growth. Filtering performance comparison between the FRR zero-phase filter and the conventional one (using the fourth-order digital Butterworth low pass filter mentioned above) is provided in figure 7. It can be observed that there are notable transient distortion and phase shift at the start of the DR curve from the conventional low pass filter. Comparisons between the DR curves from the traditional method (using the instantaneous voltage and current at peak current point in each half cycle) and the proposed method were also carried out. To get the peak current point of each consecutive half cycle accurately, a series of zero crossing points on the welding current signal were found firstly and the results are shown in figure 8.

As shown in each subfigure of figure 9, two DR curves are very similar and there is no significant phase shift between these two curves. Notably, the DR curve from the new method can provide more detailed information about the resistance changes over time. It should be noted that two curves in figure 9(d) are from a certain welding process with expulsion. In each curve, a sudden drop can be seen and this phenomenon can be used to monitor expulsion.

4. Error analysis for the newly proposed method

To get the specific performance index of the proposed method, error analysis is necessary. Therefore a series of lapping

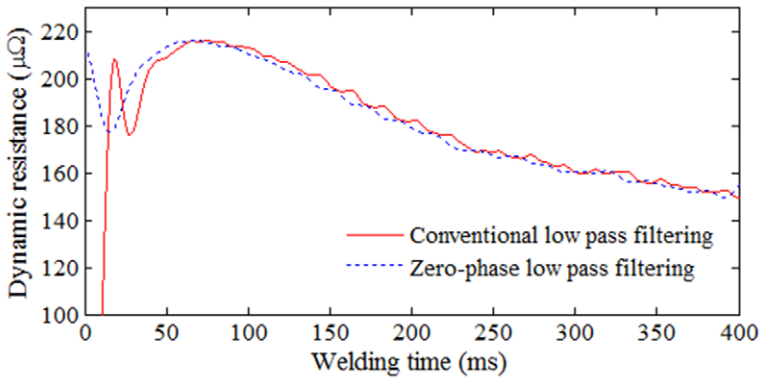

Figure 7. Filtering effect comparison.

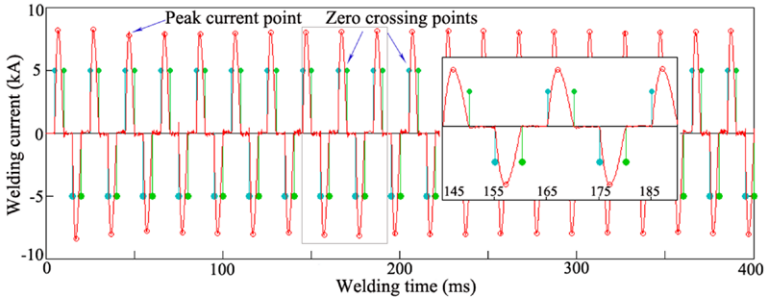

Figure 8. Zero crossing points and peak current points of the welding current.

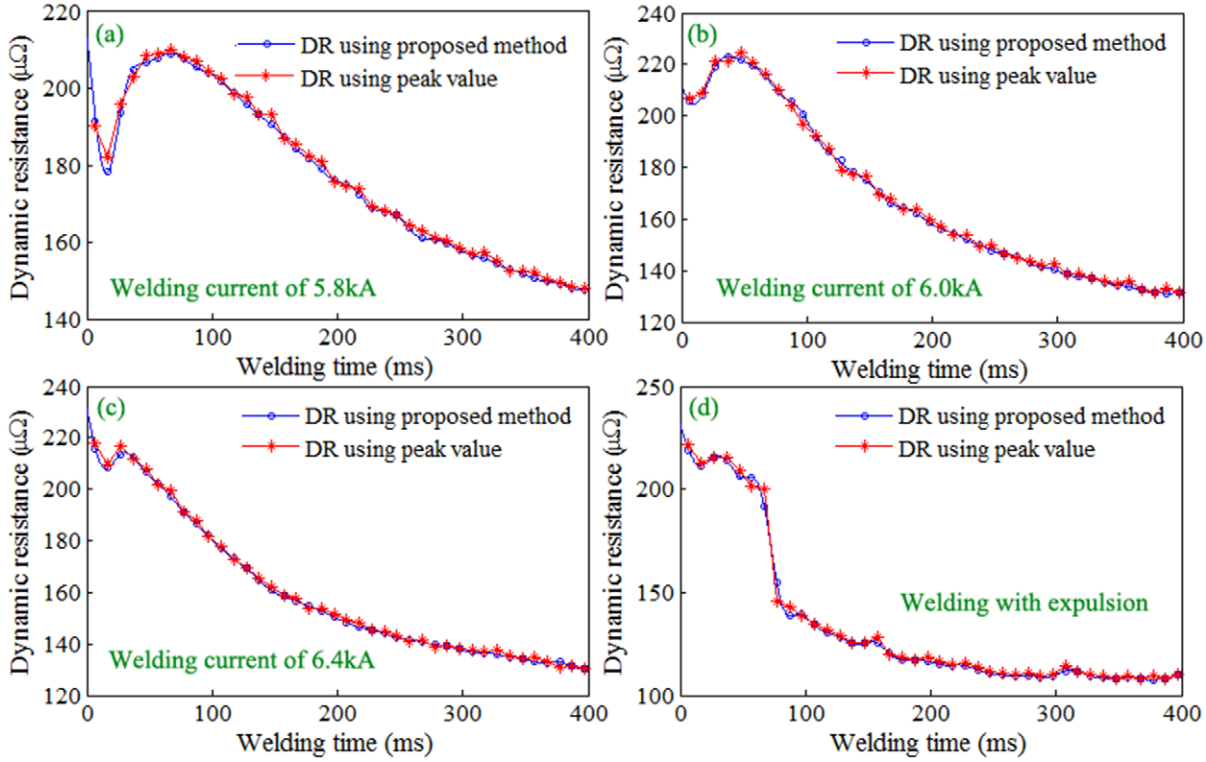

Figure 9. Comparisons of the DR curves from different methods. (a) Welding current of 5.8 kA, (b) welding current of 6.2 kA, (c) welding current of 6.4 kA and (d) welding with expulsion.

welding experiments under four welding current levels (5.4 kA, 5.8 kA, 6.2 kA and 6.4 kA) were performed. An uncoated low carbon steel sheet with a thickness of 0.7 mm was used and cut to a size of 120×30 mm^2 by laser cutting in order to get good surface flatness and edge finishing. During the welding experiments, the electrode force was set as 1.2 kN

and the welding time as 400 ms. The measurement error is defined as the difference between the measured value and true value. Because it is difficult to get the true value in most instances, the conventional true value is commonly used for error calculation instead of the true value. Generally, the average of some of the measurements is often viewed as the conventional true value, so, to evaluate the measurement error of the newly proposed method, the first thing we need to do is to get the average of some of the measurements. For each welding current level, ten DR curve samples from the traditional peak value algorithm were selected to calculate the mean curve. Additionally, ten DR curves from the welding processes with expulsion were also considered. The mean DR curves corresponding to welding currents of 5.8 kA, 6.2 kA and the welding process with expulsion are displayed in figure 10, where ten curves used for average calculation are shown as well. These means that DR curves will be used as the conventional true value for the error analysis.

In dynamic measurements, the population mean, population standard deviation and limit error are widely used parameters for random error evaluation. The population mean of n measured series can be calculated by

$$m_{ri} = \frac{1}{n}\sum_{l=1}^{n} e_{rli} \quad i = 1, 2, \ldots, m \tag{18}$$

where m is the data length of the measured series. e_{rli} represents the random error of the ith measurement in the lth measured series. The population standard deviation can be calculated by

$$\sigma_i = \sqrt{\frac{1}{n-1}\sum_{l=1}^{n}(e_{rli} - m_{ri})^2} \tag{19}$$

thus the population limit error can be calculated by

$$\delta_{\lim i} = k_p \sigma_i \tag{20}$$

where k_p is the confidence coefficient. From the error analysis theory, this coefficient usually takes 3, which means the probability of the measurement random error within $\pm\delta_{\lim i}$ is 99.73%.

As mentioned above, the welding time of all experiments in this research was set as 400 ms and it is equivalent to forty half welding cycles, therefore, there are forty data points on each mean DR curve. When calculating the random measurement error sequence of the newly proposed method, only some of the data points (corresponding to these forty data on the mean DR curve) can be used. Figure 11 gives the error analysis results. In each subfigure, the red dot line labeled as '①' represents the random error sequence. As ten DR curves were selected from each welding current level, there are ten such red dot lines in the figure. The blue solid line (marked as '②') in the middle of the subfigure corresponds to the population mean curve. Two black solid lines respectively labeled as '③' and '④' are the population limit error curves obtained by $m_{ri} \pm \delta_{\lim i}$. From figure 11, it can be observed that the random errors are mainly distributed in $\pm 5\ \mu\Omega$ and the population limit errors are mostly smaller than 15 $\mu\Omega$. It shows a good calculation precision.

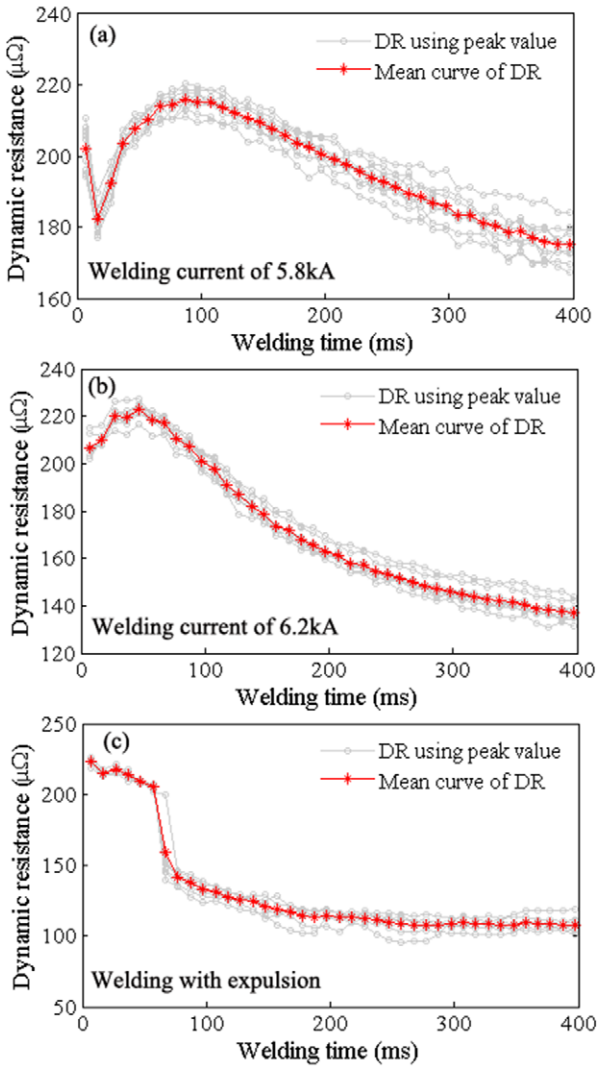

Figure 10. Mean DR curves. (a) Welding current of 5.4 kA, (b) welding current of 6.2 kA and (c) welding process with expulsion.

5. Feature extraction and discussion

The purpose of measuring and analyzing the DR signal during the RSW process is to offer positive help for welding quality monitoring. To further evaluate the effectiveness, feasibility and reliability of the newly proposed method, tensile shear strengths of the weld samples used for error analysis were tested based on the International Standard ISO 14273-2000 and a tensile-shear testing machine Zwick Roell Z020 was used. Some typical DR curves from different welding currents are shown in figure 12. Additionally, a certain DR curve with expulsion is also considered and it was monitored at 6.4 kA welding current. With the increased welding current, significant differences in the shape, slope and magnitude of the DR curves can be seen. But even so, three phases, namely rapid drop, fast rise and slow decline, still can be distinguished except the DR curve from expulsion.

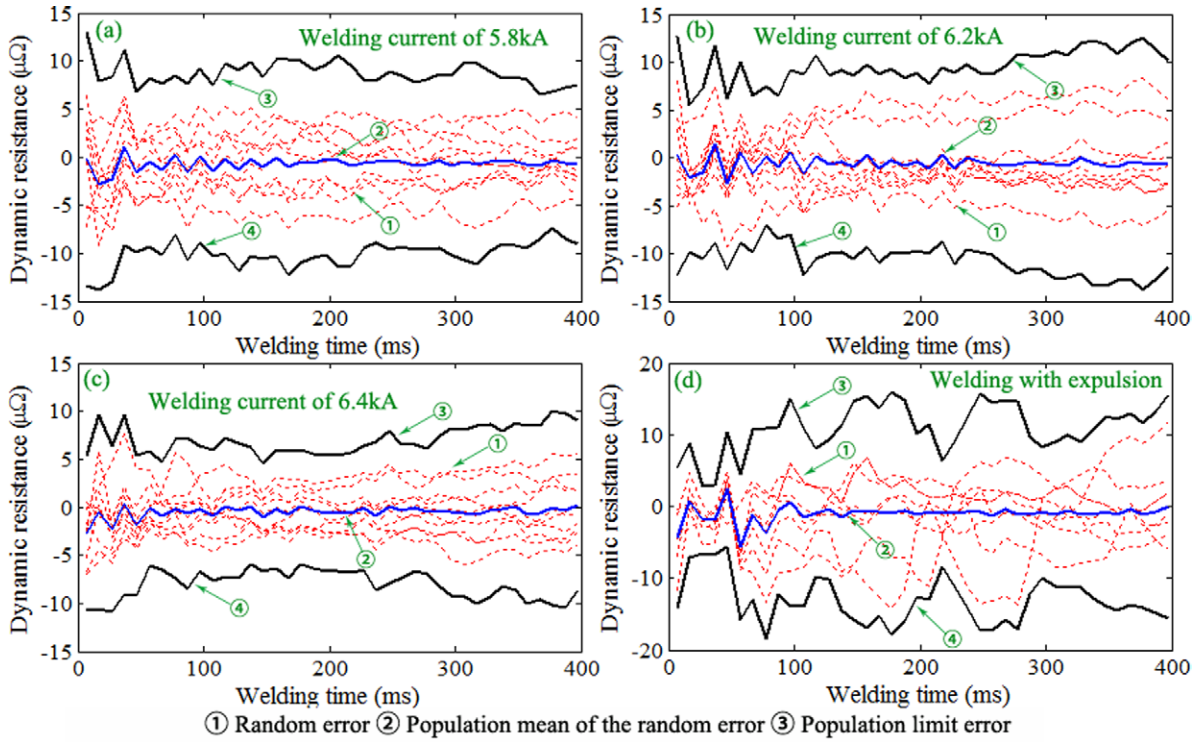

Figure 11. Error analysis results of the proposed method. (a) For welding current of 5.8 kA, (b) for welding current of 6.2 kA, (c) for welding current of 6.4 kA and (d) for welding with expulsion.

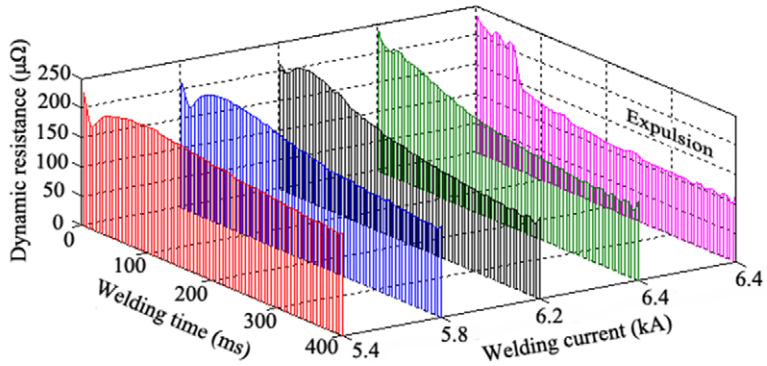

Figure 12. Dynamic resistance signals measured from different welding currents.

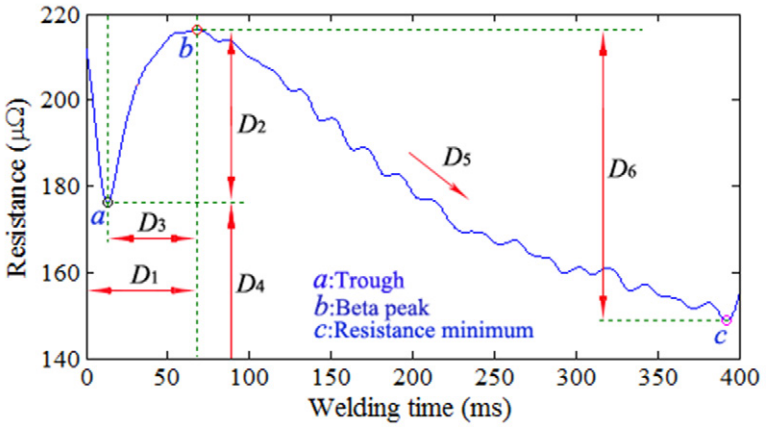

Figure 13. Schematic diagram for some extracted features.

Table 1. Descriptions and equations for the extracted features.

Features	Equation	Description
D_1	$D_1 = T_s l_b$	Beta peak time and T_s is the sampling period, l_b corresponds to the number of the sampled data between the beginning of the welding process and the beta peak point.
D_2	$D_2 = r_b - r_a$	Resistance variation between the trough a and beta peak b, $r_b$and r_a are the resistance value of the trough a and beta peak b, respectively.
D_3	$D_3 = T_s(l_b - l_a)$	Rising time corresponding to D_2, l_a is the number of the sampled data between the beginning of the welding process and trough a.
D_4	$D_4 = r_a$	Resistance value corresponding to the trough a
D_5	$D_5 = \frac{(r_b - r_c)}{[T_s(l_c - l_b)]}$	Resistance dropping rate between beta peak b and minimum resistance c, l_c corresponds to the number of the sampled data between the beta peak b and the minimum resistance point c.
D_6	$D_6 = r_b - r_c$	Resistance variation corresponding to D_5
D_7	$D_7 = \frac{1}{n}\sum_{i=1}^{n} r_i$	Mean value of the DR during the RSW process, n is the number of the sampled data
D_8	$D_8 = \sqrt{\frac{1}{n}\sum_{i=1}^{n} r_i^2}$	RMS value of the DR during the RSW process

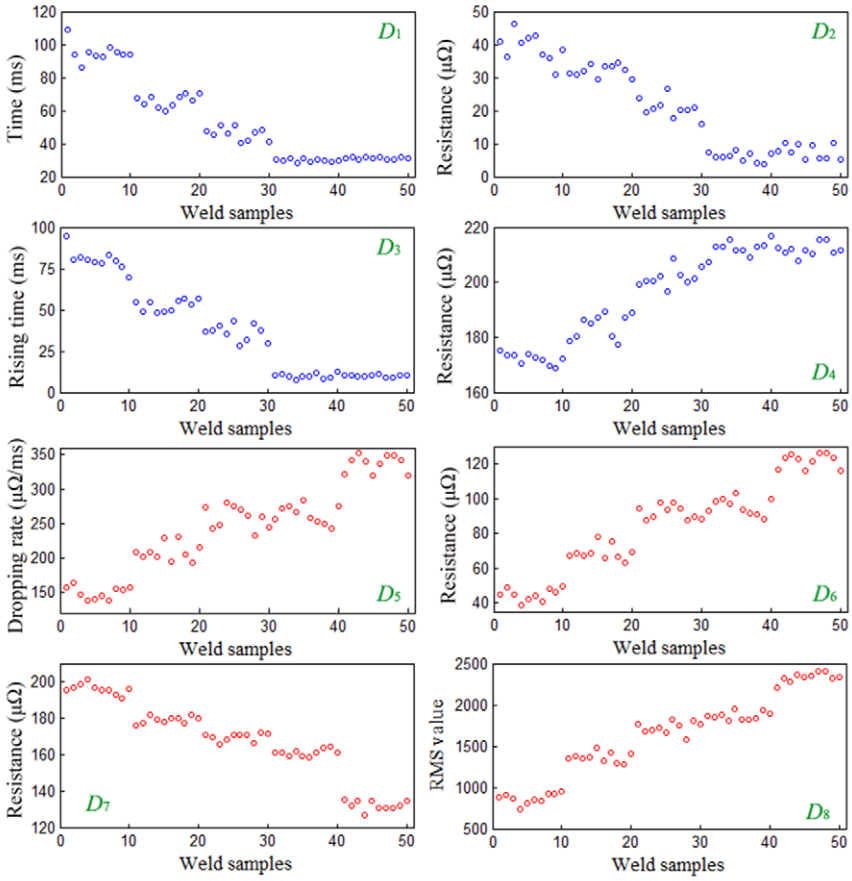

Figure 14. Scatter diagrams for the extracted features.

Then, feature extraction on the DR curves was carried out. Eight features (D_1 to D_8) in the time domain were extracted and some of them are schematically shown in figure 13, where point '*a*' corresponds to the curve trough and it is closely related to the contact resistance elimination. Point '*b*' is the beta peak and point '*c*' corresponds to the resistance minimum during the spot welding process. Detailed descriptions about the extracted features are listed in table 1.

The extracted features of the weld samples used in error analysis are shown in figure 14, where the samples from 5.4 kA are arranged at 1–10 on the horizontal axis of each subfigure, welds of 5.8 kA at 11–20, and so on. Moreover, ten welds with expulsion are assigned from 41 to 50 of the horizontal axis. As shown, with the increase of the welding current, numerical differences among the extracted features are obvious. For the welds from the normal welding process

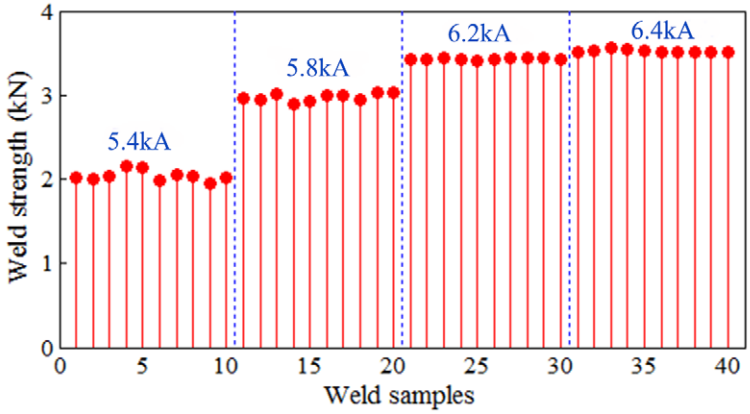

Figure 15. Measured tensile-shear strengths of the weld samples.

Table 2. Correlations between the extracted features and weld strength.

Extracted features		D_1	D_2	D_3	D_4	D_5	D_6	D_7	D_8
Weld strength	New method	−0.9593	−0.9025	−0.9203	0.9171	0.9518	0.9632	−0.9583	0.9631
	Conventional method	−0.9421	−0.9016	−0.9152	0.9002	0.9384	0.9535	−0.9417	0.9543

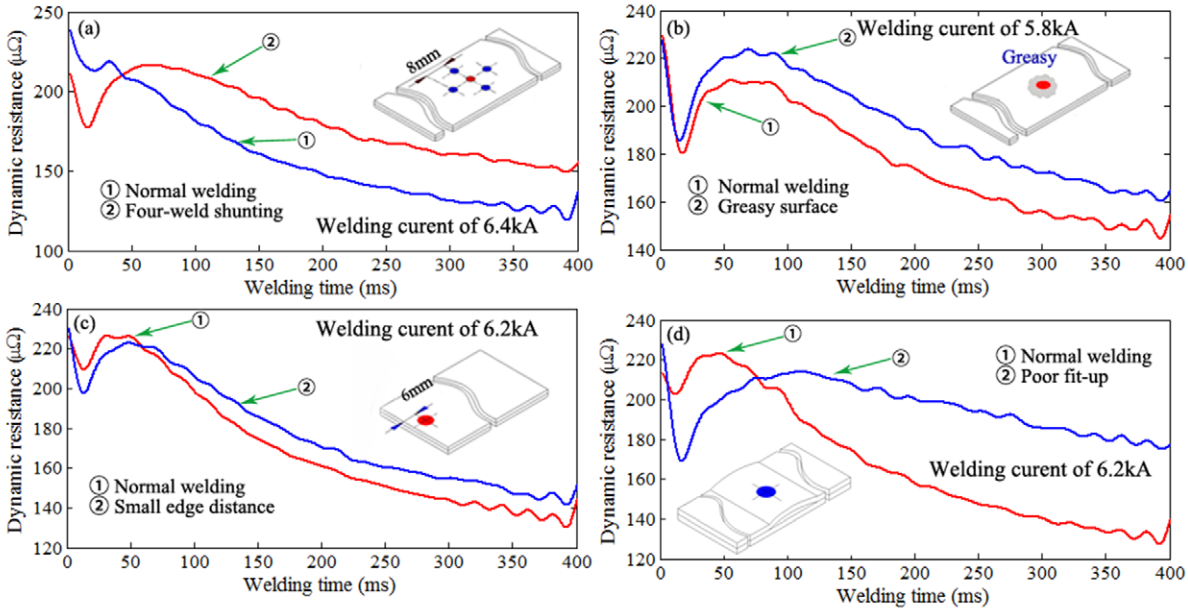

Figure 16. Comparison between the DR curves from abnormal welding and normal welding: (a) shunting, (b) greasy surface, (c) small edge distance and (d) poor fit-up.

of 6.4 kA and expulsion, the numerical differences in D_1 to D_4 are insignificant. This is because the same welding currents were adopted in these two cases, resulting in a similar changing process of the DR curves before expulsion occurs. However, features D_5 to D_8 show otherwise and they can be used to monitor expulsion.

Tensile shear strengths of these selected weld samples are shown in figure 15. It can be seen that weld strength increases with welding current. Expulsion should be avoided owing to it may decrease the energy absorption capability of the weld and destroy the corrosion resistance of coated materials, and it also consumes more energy than needed. Additionally, expulsion may severely affect surface quality and electrode life. Therefore, the strengths of the welds with expulsion are not provided in this research. The correlations between the extracted features and the weld strength were then evaluated and the results are listed in table 2. All correlation coefficients are larger than 0.9, which means these features are closely related to the weld strength and they can be used for welding quality monitoring.

The above correlation analysis results also verify the effectiveness, feasibility and reliability of the newly proposed method. In this research, features D_1–D_8 have also been extracted from the DR curves obtained by the conventional

peak value algorithm. The correlation coefficients between these extracted features and weld strength are listed in table 2 as well. It can be seen that these features also have close correlations to the weld strength. However, all correlation coefficients of the traditional method are slightly smaller than those of the new method. It can be attributed to the fact that the DR curve from the traditional method only provides limited information about the DR changes over time.

6. DR curves under abnormal welding conditions

As mentioned above, various disturbances significantly influence the spot welding process. In order to test the performance of the newly proposed method under abnormal welding conditions, several typical disturbances in the spot welding process were simulated, such as shunting, greasy surface, small edge distance and poor fit-up. DR curves from the abnormal and normal welding processes are compared in figure 16.

For shunting welding, owing to the applied welding current is shared by some shunt welds and the shunted weld, heat generation in the shunted weld is not sufficient for it to grow to the expected size. As a result, compared with the DR curve form the normal welding, the slop and amplitude of the DR curve from the shunting welding are very different, as shown in figure 16(a). It should be noted that shunting is significantly influenced by the weld spacing, surface condition, number of the shunt weld and welding schedule, among which weld spacing is the most influential factor. In order to obtain a significant shunting effect, four-weld shunting specimen is designed and the weld spacing selected in the specimen was much smaller than that in normal welding setting. Similar phenomenon can be seen in the greasy surface welding (figure 16(b)) and small edge distance welding (figure 16(c)). The weld specimen for poor fit-up welding makes reference to [5]. A poor fit-up acts as a kind of cushion when the electrode tips come into contact with the workpieces. This 'cushioning' significantly influences the contact resistance elimination as well as the nugget formation and growth. Thus, the DR curve is very different from that in normal welding, as shown in figure 16(d). Above experiments show that the DR curves from the newly proposed method can reflect the simulated abnormal disturbances well.

7. Conclusion

Based on the equivalent circuit of the spot welding machine, a new method for the DR signal acquisition has been reported in this paper. The welding voltage and current signals are measured real time and converted to analytic ones. When dividing the voltage analytic signal by the current one, the complex electrical impedance can be obtained. The real part of this complex impedance just reflects the DR changes in spot welding process. To test the effectiveness, feasibility and reliability of the proposed method, a series of welding experiments are then carried out and the tensile shear strengths of weld samples are measured. The measurement error of the newly proposed method is analyzed and the results show that the method has a good calculation precision. Several features are extracted from the DR curves obtained by the proposed method and the traditional one. Compared with the traditional method, using the instantaneous welding voltage and current at peak current point in each half cycle to calculate DR, the proposed method can provide more details of the DR changes over time. The feature extraction and correlation analysis results show that the extracted features are closely related to the weld strength and they can be used for welding quality monitoring in future studies. It also verifies the effectiveness, feasibility and reliability of the proposed method. DR curves from several abnormal welding conditions were also monitored and discussed, such as shunting, greasy surface, small edge distance and poor fit-up, the results show that the DR curves from the newly proposed method can reflect these abnormal welding processes well.

The aim of this research is to develop a new DR measurement method. In order to understand the application condition of the newly proposed method further, for future study, it would be necessary to carry out the sensitivity analysis for the proposed method. Moreover, the newly proposed method can also provide the imaginary part of the complex electrical impedance near the weldment, it would be interesting to explore the correlation between the imaginary part of the impedance and the welding quality indicator. Only uncoated low carbon steel material is selected to test the proposed method performance, some other modern steels will be further studied.

Acknowledgments

This work is supported by the Natural Science Foundation of Tianjin (Grant nos. 15JCYBJC19600 and 16JCZDJC38600). The authors would like to express their gratitude.

References

[1] Podržaj P, Polajnar I, Diaci J and Kariž Z 2008 Overview of resistance spot welding control *Sci. Technol. Weld. Join.* **13** 215–24

[2] Wang B, Lon M, Shen Q, Li Y B and Zhang H 2013 Shunting effect in resistance spot welding steels-part 1: experimental study *Weld. J.* **92** 182s–9s

[3] Li Y B, Wang B, Shen Q, Lou M and Zhang H 2013 Shunting effect in resistance welding steels-part 2: theoretical analysis *Weld. J.* **92** 231s–8s

[4] Zhang H J, Hou Y Y and Zhang J Y 2015 A new method for nondestructive quality evaluation of the resistance spot welding based on the radar chart method and the decision tree classifier *Int. J. Manuf. Technol.* **78** 841–51

[5] Wang X F, Li Y B and Meng G X 2011 Monitoring of resistance spot weld quality using electrode vibration signals *Meas. Sci. Technol.* **22** 045705

[6] Podržaj P, Boris J and Simončič S 2016 Poor fit-up condition in resistance spot welding *J. Mater. Process. Technol.* **230** 21–5
[7] Zhang Y S, Wang H, Chen G L and Zhang X Q 2007 Monitoring and intelligent control of electrode wear based on a measured electrode displacement curve in resistance spot welding *Meas. Sci. Technol.* **18** 867
[8] Podržaj P, Polajnar I, Diaci J and Kariž Z 2006 Influence of welding current shape on expulsion and weld strength of resistance spot welds *Sci. Technol. Weld. Join.* **11** 250–4
[9] Zhao D, Wang Y, Lin Z and Shen S 2013 Quality monitoring research of small scale resistance spot welding based on voltage signal *ISIJ Int.* **53** 240–4
[10] Podržaj P, Polajnar I, Diaci J and Kariž Z 2004 Expulsion detection system for resistance spot welding based on a neural network *Meas. Sci. Technol.* **15** 592
[11] Simončič S and Podržaj P 2014 Resistance spot weld strength estimation based on electrode tip displacement velocity curve obtained by image processing *Sci. Technol. Weld. Join.* **19** 468–75
[12] Zhang H J, Wang F J, Xi T, Zhao J and Wang L J 2015 A novel quality evaluation method for resistance spot welding based on the electrode displacement signal and the Chernoff faces technique *Mech. Syst. Signal Process.* **62–3** 431–43
[13] Zhang H J, Wang F J, Gao W G and Hou Y Y 2014 Quality assessment for resistance spot welding based on binary image of electrode displacement signal and probabilistic neural network *Sci. Technol. Weld. Join.* **19** 242–9
[14] Simoncic S and Podrzaj P 2012 Image-based electrode tip displacement in resistance spot welding *Meas. Sci. Technol.* **23** 1–7
[15] Podržaj P, Polajnar I, Diaci J and Kariž Z 2005 Estimating the strength of resistance spot welds based on sonic emission *Sci. Technol. Weld. Join.* **10** 399–405
[16] Podržaj P and Simončič S 2013 Resistance spot welding control based on the temperature measurement *Sci. Technol. Weld. Join.* **18** 551–57
[17] Li Y B, Xu J, Chen G L and Lin Z Q 2005 Real-time measuring system design and application of thermal expansion displacement during resistance spot welding process *Proc. SPIE* **6041** 60411T
[18] Wang X F, Li Y B, Li R H and Meng G X 2013 Experimental study on electrode displacement fluctuation characteristics during resistance spot welding *Sci. Technol. Weld. Join.* **16** 140–5
[19] Chied C S and Kannatey-Asibu Jr E 2002 Investigation of monitoring systems for resistance spot welding *Weld. J.* **81** 195s–9s
[20] Cho Y and Rhee S 2003 Experimental study of nugget formation in resistance spot welding *Weld. J.* **82** 195s–201s
[21] EI Ouafi A, Bélanger R and Méthot J F 2011 Artificial neural network-based resistance spot welding quality assessment system *Metall. Res. Technol.* **108** 343–55
[22] Zhou K and Cai L L 2013 Online nugget diameter control system for resistance spot welding *Int. J. Manuf. Technol.* **68** 2571–88
[23] Wei P S, Wu T H and Chen L J 2013 Joint quality affected by electrode contact condition during resistance spot welding *IEEE Trans. Compon. Packag. Manuf. Technol.* **3** 2164–72
[24] Savage W F, Nippes E F and Wassell F A 1978 Dynamic contact resistance of series spot welds *Weld. J.* **57** 43s–50s
[25] Gedeon S A, Sorensen C D, Ulrich D T and Eagar T W 1987 Measurement of dynamic electrical and mechanical properties of resistance spot welds *Weld. J.* **66** 378s–85s
[26] Kaiser J G, Dunn G J and Eager T W 1982 The effect of electrical resistance on nugget formation during spot welding *Weld. J.* **61** 167s–74s
[27] Dickinson D, Franklin J E and Stanya A 1980 Characterization of spot welding behavior by dynamic electrical parameter monitoring *Weld. J.* **59** 170s–6s
[28] Graza F J and Das M 2000 Identification of time-varying resistance during welding *IEEE Instrumentation and Measurement Technology Conf. (IMTC)* 3 pp 1534–9
[29] Cho Y and Rhee S 2000 New technology for measuring dynamic resistance and estimating strength in resistance spot welding *Meas. Sci. Technol.* **11** 1173
[30] Cho Y and Rhee S 2002 Primary circuit dynamic resistance monitoring and its application to quality estimation during resistance spot welding *Weld. J.* **81** 104s–11s
[31] Luo Y, Rui W, Xie X J and Zhu Y 2016 Study on the nugget growth in single-phase AC resistance spot welding based on the calculation of dynamic resistance *J. Mater. Process. Technol.* **229** 492–500
[32] Wong Y R and Pang X 2014 A new characterization approach of weld nugget growth by real-time input electrical impedance *Engineering* **6** 516–25
[33] Tan K K, Dou H, Chen Y Q and Tong H L 2001 High precision linear motor control via relay-tuning and iterative learning based on zero-phase filtering *IEEE Trans. Ctrl. Syst. Technol.* **9** 244–53
[34] Gustafsson F 1996 Determining the initial states in forward-backward filtering *IEEE Trans. Signal Process.* **44** 988–92